Computers and Concrete, Vol. 5, No. 2 (2008) 117-134
DOI: http://dx.doi.org/10.12989/cac.2008.5.2.117

Deep-beams with indirect supports: numerical modelling and experimental assessment

Mário Pimentel*

LABEST, University of Porto, Faculty of Engineering, Rua Dr. Roberto Frias s/n 4200-465 Porto, Portugal

Paulo Cachim‡

University of Aveiro, 3810-193 Aveiro, Portugal

Joaquim Figueiras‡†

LABEST, University of Porto, Faculty of Engineering, Rua Dr. Roberto Frias s/n 4200-465 Porto, Portugal

(Received February 5, 2007, Accepted March 11, 2008)

Abstract. An experimental and numerical research was conducted to gain a deeper insight on the structural behaviour of deep-beams with indirect supports and to assess the size effects in the ultimate state behaviour. The experimental campaign focused on the influence of the reinforcement tie distribution height on the compression check of the support region and on the benefits of using unbonded prestressing steel. Three reduced scale specimens were tested and used to validate the results obtained with a nonlinear finite element model. As a good agreement could be found between the numerical and the experimental results, the numerical model was then further used to perform simulations in large scale deep-beams, with dimensions similar to the ones to be adopted in a practical case. Two sources of size effects were identified from the simulation results. Both sources are related to the concrete quasi-brittle behaviour and are responsible for increasing failure brittleness with increasing structural size. While in the laboratory models failure occurred both in the experimental tests as well as in the numerical simulations after reinforcement yielding, the numerically analysed large scale models exhibited shear failures with reinforcement still operating in the elastic range.

Keywords: non-linear analysis; non-linear fracture mechanics; deep-beams; shear; strut-and-tie models; size effects; unbonded post-tensioning.

1. Introduction

The present study is motivated by a practical problem of deep beams with indirect supports associated with the design of a compact water treatment plant located in an urban context. One of the proposed solutions consisted of an arrangement of rectangular reservoirs over which were

* Research Assistant, E-mail: mjsp@fe.up.pt
‡ Associate Professor, E-mail: E-mail: pcachim@ua.pt
‡† Professor, Corresponding Author, E-mail: jafig@fe.up.pt

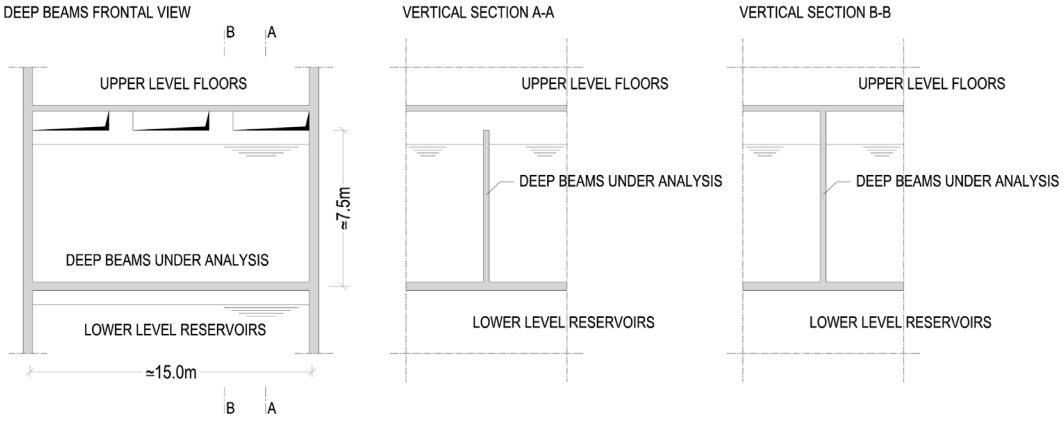

Fig. 1 Schematic layout of the deep beams in the water treatment plant design proposal

located several floors of the remaining building (see Fig. 1). Due to constraints related to the flow of the liquid between adjoining reservoirs, the loads from the upper level floors were transmitted to the lower level reservoirs by short reinforced concrete columns. The walls of these reservoirs were actually 15m span deep beams supported by orthogonal walls, with 7.5 m high, suspending the 10m span bottom slab and receiving the concentrated loads from the columns.

Due to the large dimensions of the deep-beams, to the magnitude of the involved loads, to the serviceability requirements and to the degree of repetition of this structural element along the whole structure, a refined study was undertaken in order to gain a better insight on the structural behaviour of deep-beams with indirect supports.

2. Research significance

2.1. Design procedure with equilibrium models

Deep beams are a common structural element in civil engineering where shear forces play a major role in the safety assessment. Increased complexity is recognized within the design process of wall structures when shear failures are expected. The verification to the ultimate limit states is usually accomplished using mechanical models that represent equilibrium systems of internal forces under ultimate design conditions and disregard the explicit satisfaction of compatibility conditions. The key factor in this process is to ensure the ductility that allows for internal stress redistributions, enabling the structure to adapt itself to a wide range of external loading conditions and to fulfil the idealized equilibrium scheme.

In the case of deep-beams, the design procedure prescribed in recent design codes (CEN 2004, CEN 2005) is based on strut-and-tie models (fib 1999b, Schlaich and Schafer 1991, Schlaich, *et al.* 1987). This is a plasticity based equilibrium method wherein the compatibility conditions are not directly satisfied. Strain incompatibility of struts and ties is indirectly considered by selection of appropriate angles between them. To ensure the required ductility, besides care in the detail of the main reinforcement, a distributed reinforcement mesh needs to be placed over the entire beam and crushing of concrete in the nodal regions is to be assessed using conservative values. In order to

reduce the ductility demands, the elastic stress path should be closely followed (Schlaich, *et al.* 1987). Normally the serviceability checks are performed using the reinforcement stresses calculated from the equilibrium model.

2.2. Use of unbonded reinforcement and indirect supports

In the design with strut and tie models, concrete crushing must be checked in the nodal zones. When analysing deep beams, the critical node is often located in the support region. Based on compression field theories (Belarbi and Hsu 1995, Vecchio and Collins 1986, 1993) the strength adopted for the struts is reduced because the compression field is crossing cracks and must account for the reduction of the strut width due to rough crack surfaces, disturbances caused by reinforcing bars crossing the strut, bond induced transverse tension and slip of the crack faces. The use of unbonded prestress steel could be beneficial in the sense that, in the absence of bond, less cracks would occur near the support and the overall integrity of the concrete could be improved. Also the formation of shear cracks could be delayed, increasing the beam resistance to shear failures. A similar idea has already been expressed in Muttoni and Schwartz (1991). This effect can only be assessed with the appropriate compatibility conditions and using realistic material laws through numerical analysis.

In the case of deep-beams with indirect supports, the stress flow is influenced by the existence of a stiffer and enlarged support. However, it is common practice to design this type of structures using the same strut-and-tie models used for the design of regular deep-beams, neglecting the effect of the indirect support in the compression check of the diagonal strut.

2.3. Size effect

When dealing with large structural elements, size effects should also be taken into account during the design process. Many possible sources of size effects have been identified and for a brief discussion see Tan and Cheng (2006). In this work size effects will be discussed from a fracture mechanics point of view. In the case of tension cracks propagation, it is suggested that size effects occur whenever the minimum reinforcement ratio $\rho_{MIN} \approx f_{ct}/f_{yk} \approx 0.4-0.7\%$ is not present to ensure regular crack spacing and prevent crack localization, as it is known from the fracture mechanics energy balance laws (Bazant 1984, 1999, 2001, Tommaso 1989). Since the reinforcement ratio prescribed by the Eurocode 2 over the beams height ($\rho_W = 0.2\%$) is smaller than ρ_{MIN}, size effects related to crack propagation are prone to occur.

Still within the fracture mechanics point of view, another source of size effects that was shown to be essential to describe the effect of structural size on shear failures is related to concrete crushing (Bazant 1997). Whenever the level of confinement is low, crushing of concrete is also a localized phenomena (Jansen and Shah 1997, Markeset and Hilleborg 1995, Van Mier 1986, Vonk 1993). According to experimental observations on cylindrical specimens (Jansen and Shah 1997) in the post peak range, the deformations localize in a band with a length of 2.5 to 3.0 times the cylinder diameter. As in the tension case, energy dissipation occurs at a finite region of the structure and failure becomes more brittle with increasing structural size. This fact deserves attention because the theoretical background of the plasticity methods used in the design of concrete structures is based on the assumption (not verified) of the normality rule and in the existence of a long yield plateau of compressed concrete. The latter justifies the consideration of a constant stress distribution through

the concrete struts, per example. However, as concrete is a strain softening material, failure occurs progressively, the more so the larger the structure. In this way less stress redistribution occurs at the crushed regions and the ductility requirements for the struts may not be accomplished.

It must be emphasized that this localization band length is not solely dependent on material properties, as it is commonly accepted to occur with the localization process in the tensile cracks formation. A structural behaviour is introduced because the localization band size depends on the element thickness, in the case of a laminar structure, or on the diameter, in the case of a compressed cylinder. Compressive failure is also a three-dimensional process, highly sensitive to the boundary restraint influences. It is easily understood that the degree of confinement provided by the structure strongly influences the development of this localized deformations region.

Size effects are particularly relevant since design rules are often established based on experimental evidence in laboratory tests. The dimensions of the structural elements tested in laboratory conditions are small or moderate due to equipment constraints and only a narrow band of structural dimensions can be assessed. In some full scale tests referred in the literature, strong size effects have been found, mainly related with brittle shear failures (An, *et al.* 1997, Bazant and Kazemi 1991, Collins and Kuchma 1999, Kani 1967, Walraven and Lehwalter 1991). For a complete reference list refer to Bazant and Yu (2005a, 2005b).

Size effects related to the compression failure of concrete elements are less documented. Attention as been paid to their influence on the rotation capacity of plastic hinges (Bigaj and Walraven 2002). In Ozbolt, *et al* (2000) is described a numerical and experimental work to study flexural failures of over reinforced beams of different sizes and different concrete types. Although the larger specimens had only twice the smaller specimens size, a size effect in the post peak response, and consequently on the ductility of the structure, was reported. In Bazant, *et al.* (1994) a complete review of experimental evidence of size effects on many different kind of structural failures is presented.

2.4. Objectives

In this work, the performance of a numerical model, available in the finite element code DIANA, is assessed in the evaluation of the structural response of deep beams tested in the laboratory. With the aid of this numerical model is intended to gain some insight on the way the load is carried through structures of this kind, to evaluate the design procedures based on strut-and-tie models, to examine the stress flow in the support region, to assess the effect of structural size on the failure modes and to suggest some detailing recommendations.

3. Numerical model

3.1. Model outline

The numerical model is currently implemented in the finite element code DIANA being referred in the program documentation (Witte and Kikstra 2005) as the ‘multi-directional fixed crack model’. Details about the model and its implementation issues can be found in Borst (1987), Borst and Nauta (1985), Rots and Blaauwendraad (1989). A plasticity formulation is used for the compression domain while a smeared crack model with strain decomposition within a local strain concept is used for the tension domain. This model uses an implicit formulation as the total strain is the sum of an

elastic ε_e, plastic ε_p and crack ε_{cr} components and an internal iterative procedure is needed for their calculation in each load step.

The model allows for multiple cracking in the same integration point, which is an important feature for reproducing crack propagation in beams with higher shear span ratios, *l/d*, than the analysed deep beams (Pimentel 2004) or failures due to complex load histories (Maekawa, *et al.* 2003). The maximum number of cracks per integration point is defined by the threshold angle α. As in present case multiple cracking is not essential to reproduce the expected crack patterns, the default value of α=60º was used.

A crack is formed when both the tension cut-off is violated and the angle between the potential new crack and an eventual existing crack exceeds the threshold angle α. In the case of localized crack propagation, a fracture energy based bi-linear tension softening diagram was used in this study to define the stress-strain relation after cracking. The crack band width *h* is related to the type and size of the finite element and crack orientation. Eight replace "nodded" by "node" second order plane stress elements were used and *h* was calculated according to Dahlblom and Ottosen (1990).

The reinforcement was modelled with an embedded formulation. The displacements of the reinforcement element nodes are interpolated from the mother concrete elements nodal displacements. Bond interaction between concrete and reinforcement was modelled in this study with an averaged approach using the tension stiffening diagram proposed in Figueiras (1983), relating the average tensile Replace "strength" by "stress" carried by concrete with the average strain of the reinforcement. Tension stiffening was assumed in the finite elements with a reinforcement ratio larger than ρ_{MIN}. After cracking the current version of the model only allows the definition of a constant shear retention factor, β. In this study a constant shear retention factor $\beta = 0.1$ was adopted.

In the current version of DIANA, the Drucker-Prager or Mohr-Coulomb yielding surfaces are proposed for combination with the smeared-crack model. For the compression domain it was selected the Drucker-Praguer failure surface with an associated flow rule. The best fit to the biaxial compression failure envelope of concrete is obtained with a friction angle $\phi = 10^o$ and a cohesion c=0.42f_c. The uniaxial strain hardening diagram is user-defined. The ascending was defined to fit the uniaxial curve proposed by the CEB (CEB 1993, fib 1999a) and the softening branch was defined according to the compressive damage zone model of Markeset and Hillerborg (1995).

Compressive strength in the finite elements crossed by a diagonal compression field and with a bonded reinforcement ratio larger than the minimum was reduced to 0.85f_{cm}, according to Reineck (1991, 1995), to account to the strut width reduction due to rough crack surfaces, disturbances caused by reinforcing bars crossing the strut and bond induced transverse tension. The slip along crack surfaces is already accounted for in the model, and the use of the compressive strength relations proposed by the usual compression field theories would be incorrect, as recognized in Vecchio (2000), and should be used only in co-rotational formulations (rotating crack models).

It was also intended to assess if the structural response could be reproduced using the standard material parameters values as recommended by the MC90 (CEB 1993) for normal strength concrete. In this way, it was possible to evaluate the utility of the numerical model to perform analysis in the design stage of this kind of structures. All the remaining model parameters, f_{ct} and G_F, were therefore calculated from the compressive strength, f_c, following the MC90 guidelines.

3.2. Numerical procedure

A displacement-controlled incremental loading was applied in the finite element analyses. The

adopted iterative procedure was the BFGS secant stiffness method. A tolerance defined as 0.01% of the energy norm was used as convergence criterion. This procedure was found to be reliable and robust within other applications of this model in the analysis of reinforced concrete structures (Pimentel 2004).

The major drawback in this kind of numerical analysis, mainly with smeared crack models implicit formulations, is the difficulty in finding converged solutions near collapse. As pointed out by Borst and Nauta (1985) a divergence in the iterative solution procedure can not be simply identified as physical failure. In this work either converged solutions in softening regime of the load/displacement diagram are found to identify a structural failure or physical explanations are presented to justify the divergence of the iterative procedure.

4. Experimental program

Three specimens were tested, with the geometry and reinforcements presented in Fig. 2. The specimens were designed using strut-and tie models, in such a way that reinforcement yielding should occur just before concrete crushing. In all specimens the distributed reinforcement ratio remained approximately constant, and the distribution of steel in the main tie was varied. In model

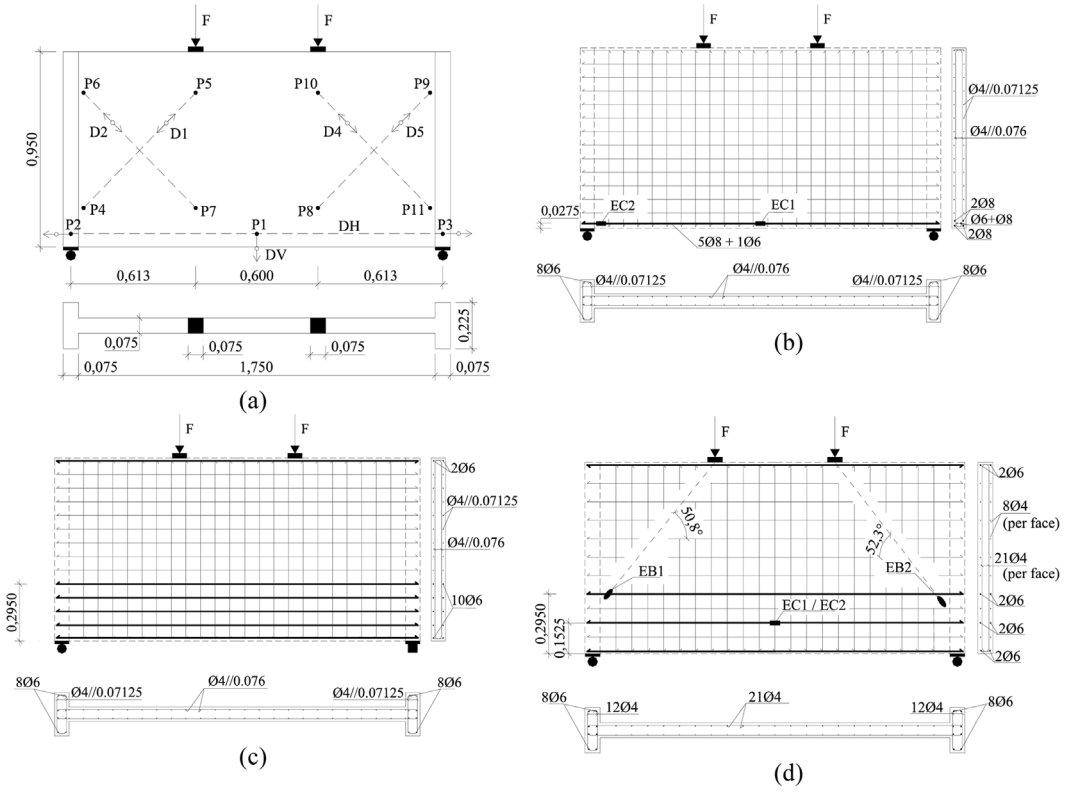

Fig. 2 (a) Dimensions of the tested specimens; (b) Reinforcement plan of model M1; (c) Reinforcement plan of model M2; (d) Reinforcement plan of model M3 (without the pre-stressing wires)

Table 1 Material properties

Model	Concrete			Reinforcing steel		Prestress steel
	f_c (MPa)	f_{ct} (MPa)	G_F (N/m)	f_y (MPa)		f_y (MPa)
M1	45	3.3	75	530 (tie)	180 (web)	-
M2	38	2.9	66			-
M3	41	3.0	70			1600

M1, the main tie, with a total section of 2.80 cm^2, was concentrated over a total height of 4 cm, being considered at 2.75 cm from the bottom for equilibrium purposes. The design with a strut-and-tie model clearly states that this model does not satisfy the check for the compression failure in the support node. In model M2, the main reinforcement, with a total section of 2.83 cm^2, was distributed over 33 cm. This height was defined according to the safety check of the support node and follows closely the elastic stress distribution. In model M3 the reinforcement was placed over the same height as in the model M2 but 40% of the tie reinforcement was replaced by 2 prestressed wires with 5 mm diameter. Model M3 was first loaded without the pre-stressing wires. Then pre-stressing was applied and the beam loaded to failure.

The material properties of all the models are presented in Table 1. For the distributed reinforcement plain mild steel was used while for the ties deformed bars were used. Due to the structural dimensions and to facilitate the casting procedures, self-compacting concrete with a maximum aggregate size of d_g=10 mm was used. The compressive strengths were determined in standard 15×15×15 cm cubic specimens ($f_{c,\,cube}$) and transformed to the reference compressive strength in cylinders, f_c.

The models were instrumented with LVDT's fixed to the concrete and strain-gages glued on the main reinforcement (EC1 and EC2). In model M3 strain-gages embedded into the concrete were also used to measure concrete strains (EB1 and EB2). The loading was applied with displacement control. All the displacements were measured between internal points of the beams to minimize errors. The horizontal displacement, DH, refers to the differential displacement of P2-P3 Fig. 2(a) and the vertical one, DV, measures the mid-span deflection.

5. Results

5.1 Model M1

In the experiment, model M1 failed for an ultimate load of F=273 kN, long after reinforcement yielding, with concrete crushing under the loading platens and failure in the support region due to the localized action of the concentrated reinforcement tie (Fig. 3(a) to (c)).

The experimental and the numerical crack patterns are presented in Fig. 4 for several stages of the test. The numerical cracking pattern is represented by the cracking strain vectors and it is displayed just on half specimen. It can be seen that crack propagation is well reproduced by the numerical model. Vertical flexural cracks start to propagate at mid span and only after curved cracks propagate from the bottom of the shear span, outlining the shape of the compression struts. After reinforcement yielding a straight splitting crack occurs between the loading platen and the support.

Fig. 3 Experimental failure of model M1: (a) Overall cracking pattern before failure; (b) Detail of the support region; (c) Detail of the loading platen region

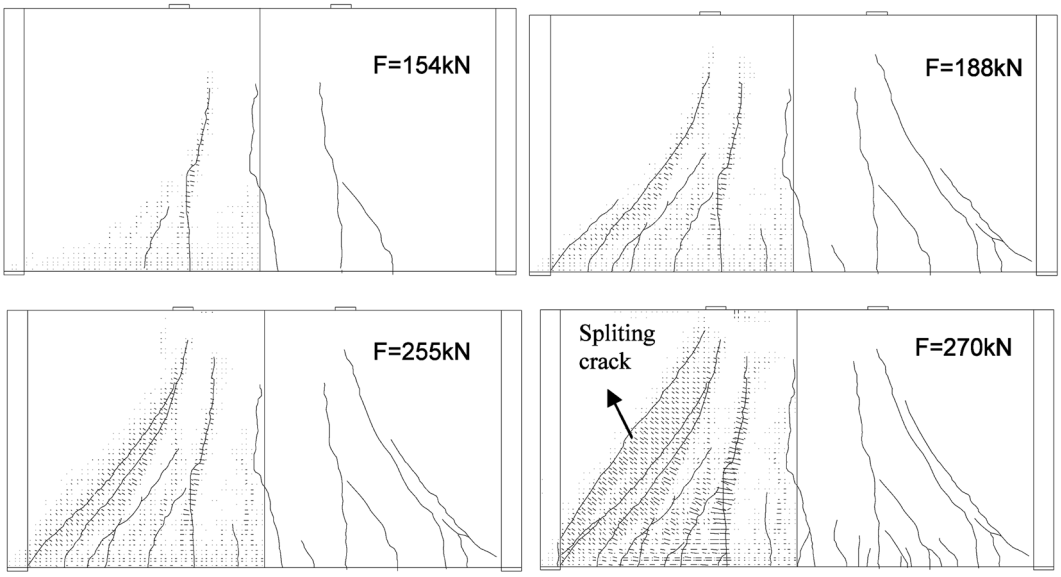

Fig. 4 Evolution of the experimental cracking pattern and computed cracking strain vectors

The evolution of the readings in the LVDTs and in the strain gages is depicted in Fig. 5 along with the corresponding numerical counterparts. In general a good fit can be observed.

The divergence of the algorithm occurred after several load steps with the concrete in the softening regime in the loading platen region and after large redistribution of the compressive stresses, similar to the observed in the experiment.

5.2 Model M2

From this test is only available the failure load and failure mode. Failure occurred for F=235 kN, after reinforcement yielding, by a shear compression mechanism. In Fig. 6(a) are presented the numerical and experimental crack patterns at failure. In Fig. 6(b) it can be observed that concrete

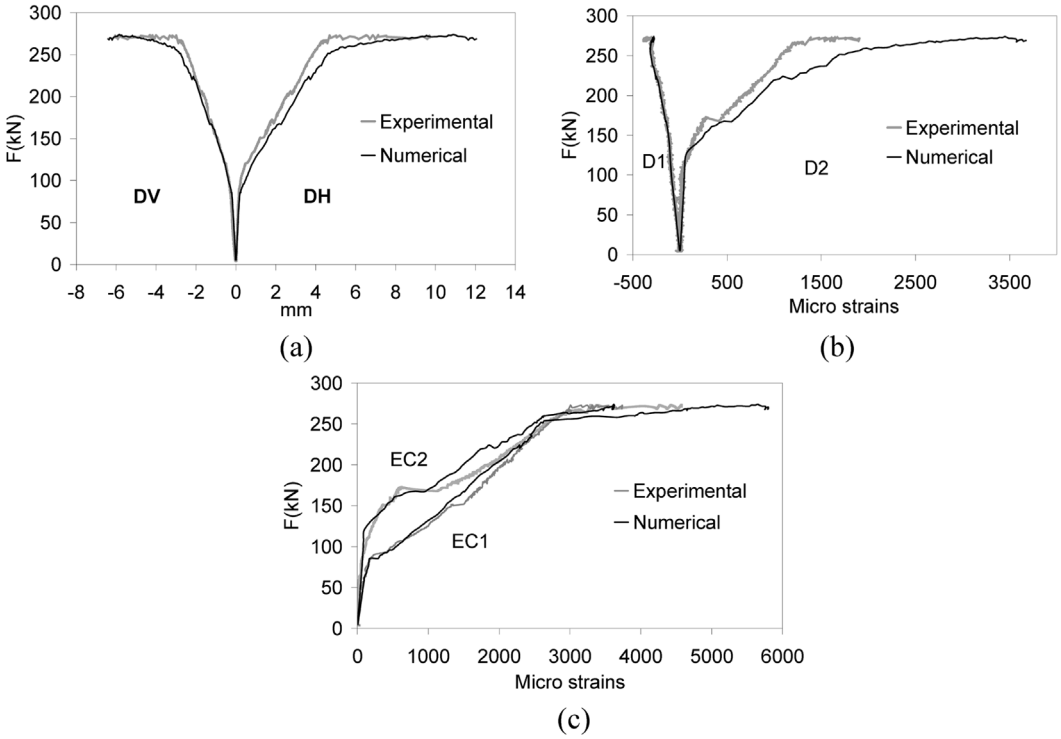

Fig. 5 Computed vs. measured deflections and strains for model M1: (a) displacements; (b) average concrete deformations; (c) steel strains

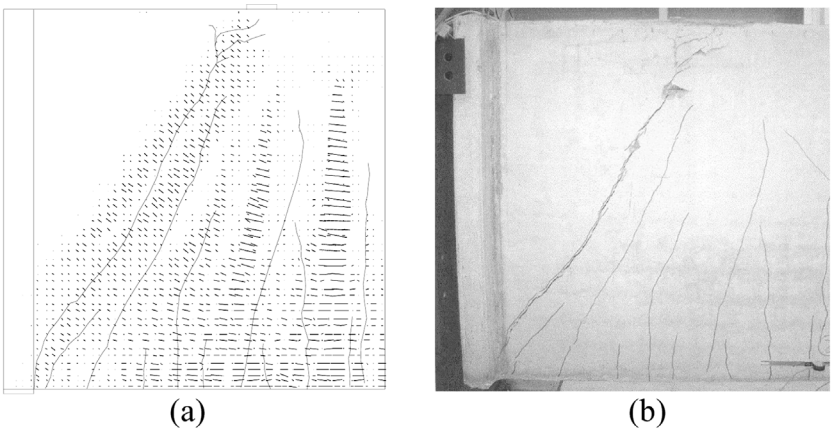

Fig. 6 (a) Experimental cracking pattern and computed cracking strain vectors at failure.; (b) Experimental failure

crushed at the shear crack tip, mainly in the outer region of the loading platen, supporting the statement made about the failure mechanism.

In Fig. 7 the computed shear strain, γ_{xy}, contours are depicted. In the numerical model shear failure is triggered by the softening regime of the concrete near the loading platen, in the shear span side, causing

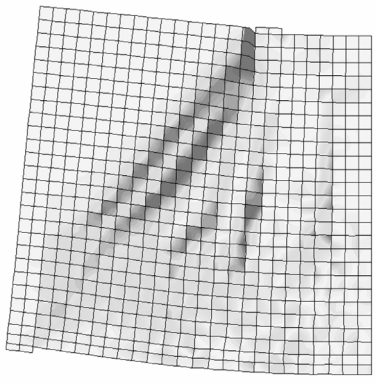

Fig. 7 Computed deformed shape with shear strain contours

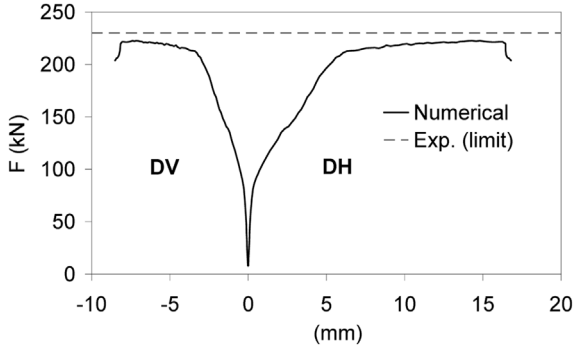

Fig. 8 Computed load-displacement diagrams for model M2

the large shear strains observed in that region. Localization along a shear band can be found, but in the region where the main reinforcement exists, no distinct localization can be seen, although the experimental crack pattern at failure clearly indicates a wide shear crack at the support region.

The numerical load displacement diagrams are presented in Fig. 8. Divergence of the algorithm occurred long after the concrete elements entered in the softening domain and after large redistribution of the compressive stresses.

5.3 Model M3

This model was first loaded without the pre-stressing wires, until a 5 mm displacement was reached in the horizontal transducer, DH. The pre-stress was applied and just before the second phase of the test it was measured a total pre-stressing force of 31 kN, corresponding to an initial stress of 790 MPa in each wire. The crack pattern after the first phase of the test, at the time of pre-stressing, is depicted in Fig. 9.

No new flexural cracks were formed after the pre-stress application. The existing flexural cracks started to propagate for a load of about 200 to 220 kN and only after the splitting cracks appeared. The ultimate load was F=246 kN and the beam failed by a flexural mechanism. A wide open flexural crack can be seen in Fig. 10. Failure was triggered by the break of a reinforcing bar that

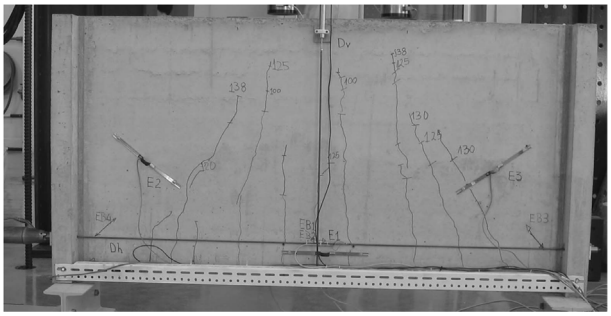

Fig. 9 View of model M3 during the pre-stress application

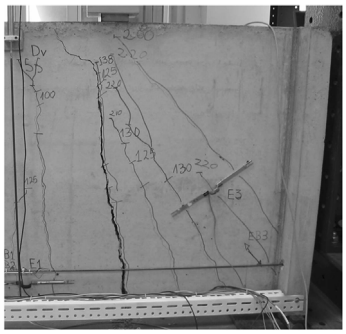

Fig. 10 Model M3 at failure

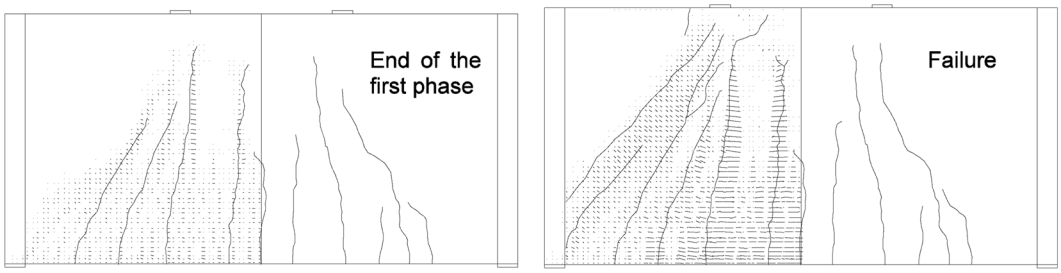

Fig. 11 Evolution of experimental cracking pattern and computed cracking strain vectors

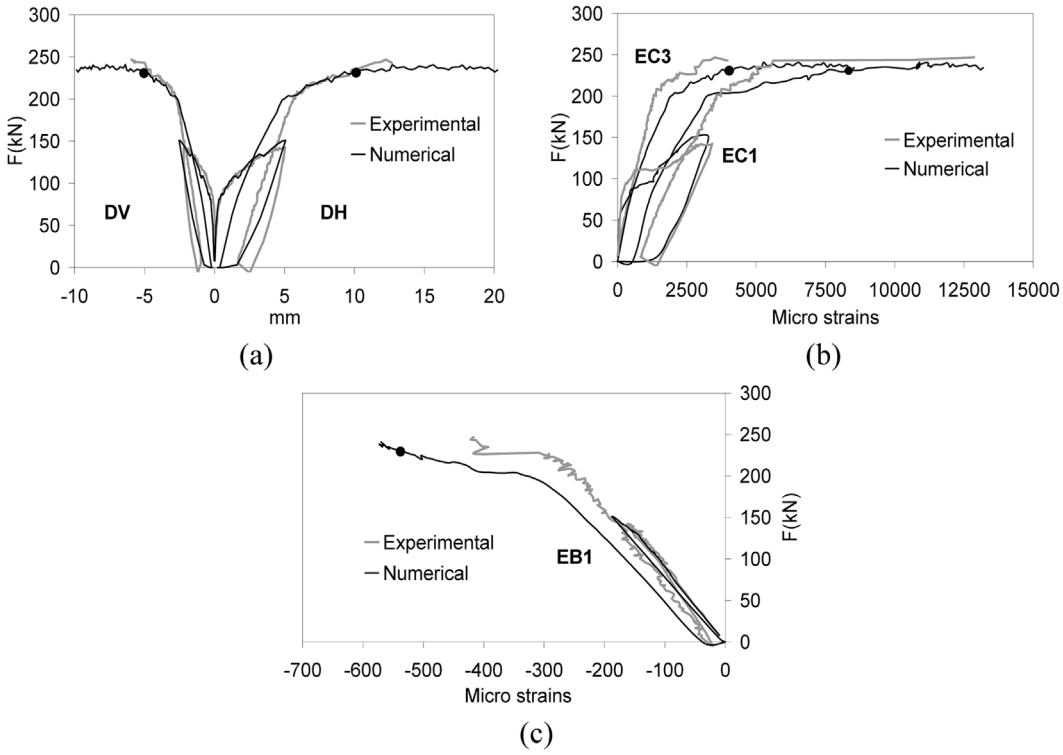

Fig. 12 Computed and measured deflections and strains for model M3: (a) displacements; (b) reinforcement (EC1) and prestressing wire (EC3) strains; (c) concrete strains

crossed the flexural crack and coincided with the pre-stressing wires yielding.

In the numerical model the prestressing force was applied as an equivalent nodal force at the anchorage location. This is a reasonable modelling assumption since the prestressing wires are unbonded. After the prestressing force application a bar element was activated for modelling the prestressing wires, enabling to capture the wire strain evolution with the loading as well as its contribution for the structural stiffness. The numerical model also predicts a flexural failure, but as the break of the reinforcing bars is not included, concrete crushing occurred in the horizontal strut, just near the loading platen. The numerical and experimental crack patterns are depicted in Fig. 11, and a good agreement can be found.

The load/deformation diagrams are illustrated in Fig. 12. In the numerical curves, the load step where the pre-stressing wires yield is marked with a dot. The unloading/reloading stiffness is slightly different from the experimental, what can be attributed to the fact that the tension model unloads and reloads with the secant stiffness, without residual cracking strains. In the evolution of the wire strains (Fig. 12(b)) it can be seen that the experimental curve has a constant slope until the existing flexural cracks started to propagate. The numerical curve presents a more gradual stiffness degradation. The readings in the reinforcement strain-gage EC1 are well predicted and also the concrete strains (EB1) were fairly reproduced by the numerical model (see Fig. 12(c)).

5.4. Discussion

All failures occurred after reinforcement yielding, and from an ultimate load point of view, it can be concluded that all the reinforcement arrangements were satisfactory. For the tested small scale models the failure loads were higher than predicted during the design stage.

5.4.1. Performance of the numerical model or remove the section number

Regarding the performance of the numerical model in reproducing the observed structural behaviour, a good agreement was found between the experimental measurements and the numerical predictions. The experimental failure modes and loads had a good correspondence with the calculated ones and the cracking propagation was accurately predicted during all the test stages. In this way the numerical results are validated and can be further used to explain the structural behaviour of the tested specimens.

5.4.2. Compression check for the diagonal strut of model M1I

Although the diagonal strut of model M1 did not fulfil the compression check during the design

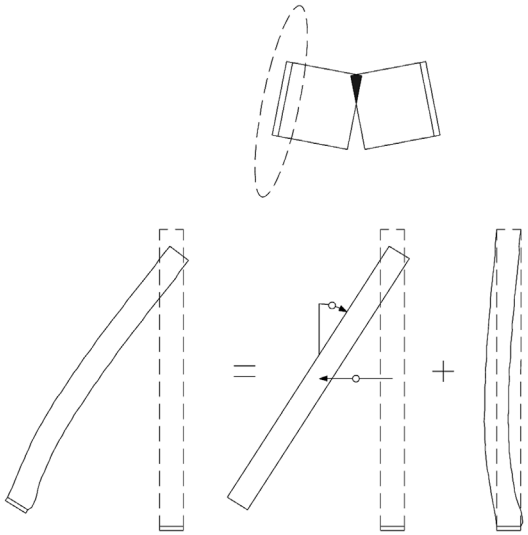

Fig. 13 Deformation of the enlarged support column

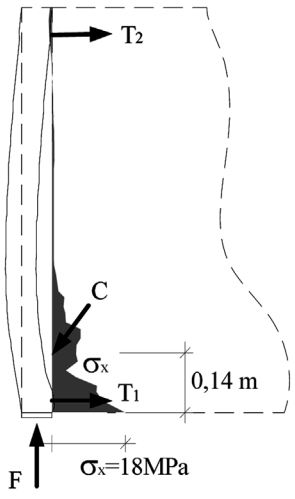

Fig. 14 Equilibrium of forces at the interface with the enlarged support column

stage at the support node, due to an extremely concentrated reinforcement arrangement, both in the test and in the numerical analysis the beam exhibited a ductile type of failure. Observing the numerical deformed shape of the enlarged support column, it is possible to divide it in a rigid body motion, consequence of the deep-beam deformed shape, and a deformation that clearly indicates bending of this column due to the compression strut action (Fig. 13).

Let us now analyse the stress flow at the vicinity of the discontinuity line between the enlarged support column and the deep-beam web (Fig. 14). From the horizontal stress distribution, Greek symbol for "s", it is possible to calculate the position of the resultant force, C, carried by the compression strut (force F is the support reaction, T1 the force carried by the bottom reinforcement and T2 is a small traction force at the top of the column as calculated from the numerical results).

In Fig. 15 is depicted the overall strut-and-tie equilibrium model that explains the stress flow in the deep-beam. The horizontal strut follows the horizontal stress distribution resultant along the symmetry axis. It can be seen that the struts, as determined from the stress distributions, suit extremely well the cracking pattern, namely the splitting crack between the loading platen and the support. It can also be seen that the direction of the diagonal compression strut does not intersect the bottom reinforcement tie, which means that the diagonal stress flow direction is further diverted inside the enlarged support region. This can be explained by the bending action of the enlarged support column, as illustrated in the equilibrium model, and is confirmed by the computed principal stress flow. This effect, although also present, it is not so pronounced in the other models where the tie is distributed over a larger height.

With the aid of this strut-and-tie model it is possible to show that, in fact, the compression check is satisfied.

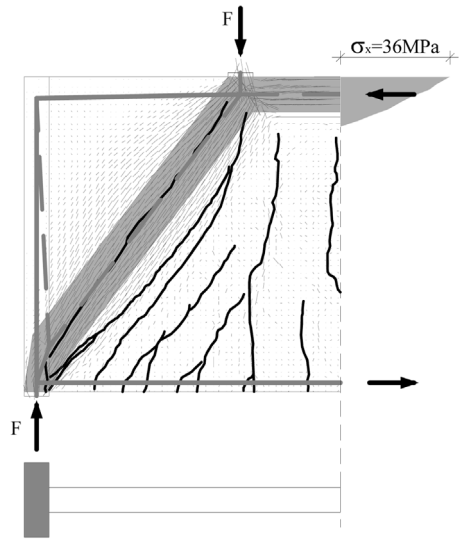

Fig. 15 Updated strut-and-tie model for M1 plotted over the computed principal compressive stresses and the experimental cracking pattern

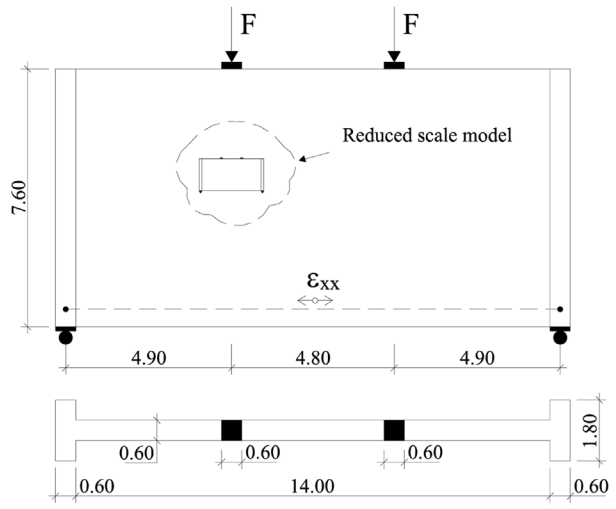

Fig. 16 Large scale beam dimensions, similar to the practical problem to be solved

5.4.3 Effect of the unbonded prestress

Comparing now the observed failure modes of model M2 and M3, the partial post-tensioned beam M3 exhibited a reinforcement failure while model M2 failure occurred due to concrete crushing following a shear/compression mechanism. It must also be remarked that, while in model M2 a continuous shear crack propagated from the bottom fibre towards the loading platen, in model M3 only splitting cracks were formed. Although only one test was carried out and despite the fact that slightly different concretes were used, the post-tensioned unbonded reinforcement seems to have a positive contribution towards the avoidance of the shear failure mechanism by improving the concrete integrity in the shear span and delaying the shear crack formation near the supports.

6. Size-effects study

Three large scale deep-beams were numerically analysed. The dimensions were obtained scaling up 8 times all the tested specimens dimensions and are close to the dimensions of the water treatment plant deep-beams (Fig. 16). The finite element mesh was similar and only the element size was increased. The reinforcement ratios and relative positions were maintained so that the large scale beams are scaled up versions of the tested specimens M1, M2 and M3.

The same concrete resistances were taken for the large scale beams, but the aggregate size was changed to reflect the real concrete that would be used to cast such large beams. In this way a maximum aggregate size of d_g=32 mm was considered. According to the MC90, the fracture energy is therefore 2.2 times higher than the fracture energy considered in the reduced scale models, and equals 160, 145 and

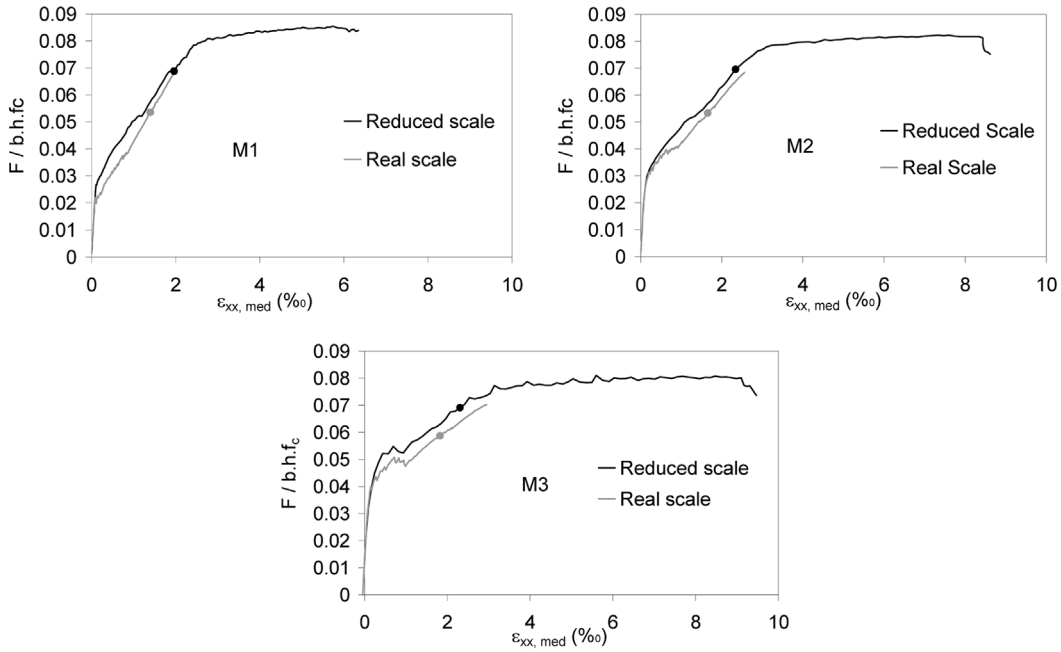

Fig. 17 Nondimensional load-deformation curves exhibiting the size-effects

155 N/m for models M1, M2 and M3, respectively. In the web, an orthogonal mesh of ϕ10//0.125 in each face was adopted, being equivalent to the mechanical reinforcement ratio ($\omega = A_s \cdot f_y / A_c \cdot f_c$) considered in the reduced scale specimens and equal to the minimum specified in the EC2 (CEN 2004).

In the case of model M3 the prestressing was now introduced before the external load was applied and an initial prestress of 1000 MPa was considered, reflecting more closely the real working stress of the unbonded prestress steel within service conditions.

The load-deformation curves are depicted in Fig. 17. As a deformation measure, the mean strain along the reference line depicted in Fig. 16 was considered. As a load measure, the nondimensional parameter $F/b \cdot h \cdot f_c$ was taken, were b and h are the beam thickness and height, respectively. This allows a direct comparison between geometrically similar beams with different scales.

A strong size effect can be observed in the load-deformation responses. In all the real scale models the obtained failure mode was similar to the one already computed for the reduced scale model M2 (see Fig. 7), but with the reinforcement in the elastic range. Concrete crushing was computed near the loading platen, in the shear span side. The computed failures can therefore be considered of brittle nature, in opposition to the observed failures in the laboratory specimens.

In the load-deformation curves of Fig. 17 the load step wherein the stress-state in one of the gauss points first reaches the compressive failure envelope is marked with a dot. In the reduced scale models, concrete in the most compressed region is already in the softening regime when the reinforcement yields. However, concrete ductility is enough to allow for stress redistributions in these highly stressed areas leading to a ductile type of failure. In the real scale models the compressive envelope is reached earlier and also stress redistributions occur allowing the load increase, but are not sufficient to achieve the reinforcement yielding.

For the same nondimensional load level, the real scale models present a more developed cracking pattern. As no minimum reinforcement is supplied in for cracking control, localized cracks propagate faster in the larger beams. This enforces the stress flow to deviate from the elastic one sooner than in the reduced scale beams, explaining the fact that the compressive envelope is reached for a lower relative load level. This can be considered as a primary source of the computed size effect. In Fig. 18 the principal stress contour levels are depicted, together with the cracking strain vectors, for the load level were the stress state reaches the compressive envelope in the large scale model M2. It can be seen that, in the real scale model, the cracking pattern is much more developed

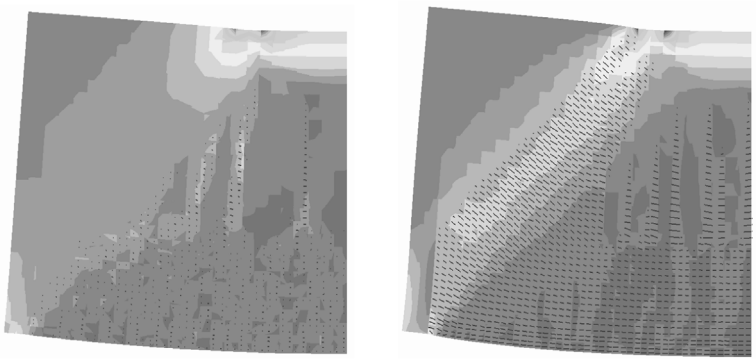

Fig. 18 Model M2 deformed shape (40x) with the principal compressive stress contours and cracking strain vectors for $F/b \cdot h \cdot f_c$ = 0.053: (a) reduced scale model; (b) real scale model

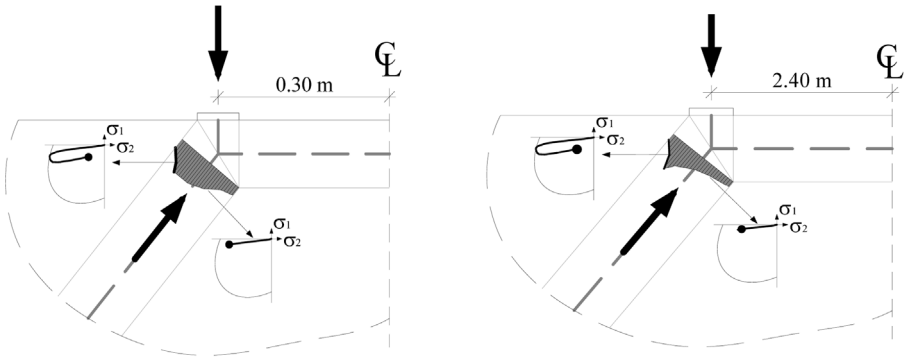

(a) Reduced Scale (b) Real Scale

Fig. 19 Principal compressive stresses in the inclined strut for model M2 at peak load: (a) Reduced scale model; (b) Real scale model

and the inclined crack tip is already near the loading platen.

The second source of the computed size effect can be found in the compressed concrete softening behaviour. In Fig. 19 the computed principal compressive stress distributions at peak load in the inclined strut are illustrated for both the reduced and real scale M2 models. In both models the relative strut section were concrete is already in the softening regime is approximately the same. However, it can be seen that in the reduced scale model a more uniform distribution is obtained, closer to the strut-and-tie model assumptions. In the real scale model, the progressive crushing of the concrete leads to the strut failure before a uniform stress distribution is attained. This fact shows that the effectiveness factor, ν, usually employed to obtain the compression strut strength, $f_c^* = \nu f_c$, from the compressive concrete strength, f_c, is size dependent. A similar conclusion has been derived theoretically in Bazant (1997).

7. Conclusions and design recomendations

From this study the following conclusions can be drawn:

- The adopted numerical model and modelling strategy provided accurate simulations of the tested deep-beams behaviour. The load-deformation curves, the failure loads and the failure modes were satisfactorily reproduced with standard model parameters. The model could be further used to gain a deeper insight in the structural behaviour of this type of beams.
- Regarding the use of unbonded prestress steel, it was shown, both numerically and experimentally, that the service behaviour is, as expected, greatly improved. Regarding the ultimate limit state behaviour, the tested prestressed specimen exhibited less cracks in the support region and consequently an improved concrete condition, delaying the shear failure mechanism. However, only one test was made and more experimental evidence is needed. In the numerical model, as failure was always triggered by concrete crushing in the node near the loading platen, no further conclusions could be drawn.
- The stress flow in the support region was explained comparing the experimental crack pattern at failure and the numerical principal compressive stress vectors. It was shown that for the beam with concentrated reinforcement (model M1), an alternative equilibrium path was formed, mobilizing the

bending stiffness of the enlarged support column and allowing the yielding load to be attained.

- If the ductility requirements are met, strut-and-tie models provide a lower bound solution for the design of deep-beams. These requirements were shown to be dependent on the structural size. In the simulations of large deep-beams, but geometrically similar to the tested specimens, two main sources of size effects related to the nonlinear fracture mechanics of concrete were found. The first is directly related to the tensile cracks propagation, which in the case of the large beams was responsible for the deviation of the stress flow from the elastic one for a lower load level. This led the concrete near the loading platen, in the shear span side, to start crushing sooner than in the reduced scale model. The other source for the computed size effect is related to the limited ductility of the concrete strut. For the large scale models, the progressive crushing of the concrete in the strut, inhibits the mobilization of the whole strut width and leads to a premature failure.

As detailing recommendations for the design of large deep-beams, the following considerations can be pointed out:

- The distributed reinforcement ratio should increase with the structural size. For large deep-beams, the effectiveness of both the bottom tie and horizontal strut in controlling the crack propagation is diminished, and cracking control reinforcement ratios closer to ρ_{MIN} should be adopted.
- In order to guarantee the ductility requirements for the compressed struts in the large beams, enabling the idealization of a constant stressed strut along its width, some extra confinement must be supplied to concrete in the nodal zones to inhibit progressive concrete crushing. Closely spaced loops may prove effective for that purpose. Otherwise the effectiveness factor should be considered size dependent.

References

An, X., Maekawa, K. and Okamura, H. (1997), "Numerical simulation os size effect in shear strength of RC beams", *J. Mater. Concrete Struct. Pavements, JSCE*, **35**, 297-316.

Bazant, Z. P. (1984), "Size effect in blunt fracture: conrete, rock metal", *J. Eng. Mech.*, **110**(4), 518-535.

Bazant, Z. P. (1997), "Fracturing truss model: size effect in shear failure of reinforced concrete", *J. Eng. Mech.*, **123**(12), 1276-1288.

Bazant, Z. P. (1999), "Size effect on structural strength: a review", *Archive of Applied Mechanics*, Springer-Verlag, Berlim, 703-725.

Bazant, Z. P. (2001), "Size effect on structural strenght", *Handbook of Materials Behaviour Models*, J. Lemaitre, ed., Academic Press, San Diego, 30-68.

Bazant, Z. P. and Kazemi, M. T. (1991), "Size effect on diagonal shear failure of beams without strirrups", *ACI Struct. J.*, **88**(3), 268-276.

Bazant, Z. P., Ozbolt, J. and Eligehausen, R. (1994), "Fracture size effect: review of evidence for concrete structures", *J. Struct. Eng.*, **120**(8), 2377-2398.

Bazant, Z. P. and Yu, Q. (2005a), "Designing against size effect on shear strength of reinforced concrete beams without stirrups: 1. Formulation", *J. Struct. Eng.*, **131**(12), 1877-1885.

Bazant, Z. P. and Yu, Q. (2005b), "Designing against size effect on shear strength of reinforced concrete beams without stirrups: 2. Verification and calibration", *J. Struct. Eng.*, **131**(12), 1886-1896.

Belarbi, A. and Hsu, T. T. C. (1995), "Constitutive laws of softened concrete in biaxial tension-compression", *ACI Struct. J.*, **92**(5), 562-573.

Bigaj, A. and Walraven, J. C. (2002), "Size effects in plastic hinges of RC members", *Heron*, **47**(1), 53-75.

Borst, R. (1987), "Smeared cracking, plasticity, creep and thermal loading - A unified approach", *Comput. Methods Appl. Mech. Eng.*, **62**(1), 89-110.

Borst, R. and Nauta, P. (1985), "Non-orthogonal cracks in a smeared finite element model", *Eng. Computations*, **2**, 35-46.

CEB (1993), CEB-FIP Model Code 1990, Thomas Telford, London.

CEN (2004), Eurocode 2: Design of concrete structures - Part 1-1: General rules and rules for buildings, Brussels.
CEN (2005), Eurocode 2 - Design of concrete structures - Concrete Bridges - Design and detailing rules, Brussels.
Collins, M. P. and Kuchma, D. (1999). "How safe are our large, lightly reinforced concrete beams, slabs, and footings?", *ACI Struct. J.*, **96**(4), 482-490.
Dahlblom, O. and Ottosen, N. S. (1990), "Smeared crack analysis using generalized fictious crack model", *J. Eng. Mech.*, **116**(1), 55-76.
fib (1999a), *Bulletin nº1: Structural Concrete. Text book on Behaviour, Design and Perfomance*, Vol. 1, fib, Lausanne.
fib (1999b), *Bulletin nº2: Structural Concrete. Text book on Behaviour, Design and Perfomance*, Vol. 2, fib, Lausanne.
Figueiras, J. A. (1983), "Ultimate load analysis of anisotropic and reinforced concrete plates and shells", PhD Thesis, University College of Swansea, Swansea, Walles.
Jansen, D. C. and Shah, S. P. (1997), "Efect of length on compressive strain softening of concrete", *J. Eng. Mech.*, **123**(1), 25-35.
Kani, G. N. J. (1967), "How safe are our large reinforced reinforced concrete beams?", *ACI J.*, **64**(3), 128-141.
Maekawa, K., Pimanmas, A. and Okamura, H. (2003), *Nonlinear Mechanics of Reinforced Concrete*, Spoon Press, London.
Markeset, G. and Hilleborg, A. (1995), "Softening of concrete in compression - Localization and size effects", *Cement Concrete Res.*, **25**(4), 702-708.
Muttoni, A. and Schwartz, J. (1991), "Behavior of beams and punching in slabs without shear reinforcement", *IABSE Colloquium - Structural Concrete*, **62**, Stuttgart, 703-708.
Ozbolt, J., Mestrovic, D., Li, Y.-J. and Eligehausen, R. (2000), "Compression failure of beams made of different concrete types and sizes", *J. Struct. Eng.*, **126**(2), 703-708.
Pimentel, M. (2004), "Modelling and analysis of concrete laminar structures: challenges and possibilities (in Portuguese)", MSc., Faculty of Engineering of the University of Porto, Porto.
Reineck, K.-H. (1991), "Modelling of members with transverse reinforcement", *IABSE Colloquium - Structural Concrete, Vol.62*, Stuttgart, 481-488.
Reineck, K.-H. (1995), "Shear design based on truss models with crack-friction", Bulletin 223: Ultimate Limit State Design Models, CEB, ed., CEB, Lausanne.
Rots, J. G. and Blaauwendraad, J. (1989), "Crack models for concrete: discrete or smeared? Fixed, multi-directional or rotating", *Heron*, **34**(1).
Schlaich, J. and Schafer, K. (1991), "Design and detailing of structural concrete using strut-and-tie models", *Struct. Eng.*, **69**(6).
Schlaich, J., Schafer, K. and Jennewein, M. (1987), "Towards a consistent design of structural concrete", *PCI-J.*, **32**(3), 74-150.
Tan, K. H. and Cheng, G. H. (2006), "Size effect on shear strength of deep beams: Investigating with strut-and-tie model", *J. Struct. Eng.*, **132**(5), 673-685.
Tommaso, A. (1989), "Size effects and brittleness", *Fracture Mechanics of Concrete Structures*, Report of the RILEM Comitee 90-FMA, L. Elfgren, ed., Chapman and Hall, London, 191-207.
Van Mier, J. G. M. (1986), "Fracture of concrete under complex stress", *Heron*, **31**(3).
Vecchio, F. J. (2000), "Disturbed stress field model for reinforced concrete: formulation", *J. Struct. Eng.*, 126(9), 1070-1077.
Vecchio, F. J. and Collins, M. P. (1986), "The modified compression-field theory for reinforced concrete elements subjected to shear", *ACI J.*, **83**(2), 219-231.
Vecchio, F. J. and Collins, M. P. (1993), "Compression response of cracked reinforced concrete", *J. Struct. Eng.*, **119**(12), 3590-3610.
Vonk, R. A. (1993), "A micromechanical investigation of softening of concrete loaded in compression", *Heron*, **38**(3), 3-90.
Walraven, J. C. and Lehwalter, N. (1991), "Size effects in short beams loaded in shear", *ACI Struct. J.*, **91**(5), 585-593.
Witte, F. C. and Kikstra, W. P. (2005), "DIANA User´s Manual - Material Library", TNO DIANA, BV, Delft.

NB